Emergent Structure of Multidislocation Ground States in Curved Crystals

Amir Azadi

Department of Physics, University of Massachusetts, Amherst, Massachusetts 01003, USA

Gregory M. Grason

Department of Polymer Science and Engineering, University of Massachusetts, Amherst, Massachusetts 01003, USA

We study the structural features and underlying principles of multidislocation ground states of a crystalline spherical cap. In the continuum limit where the ratio of crystal size to lattice spacing W/a diverges, dislocations proliferate and ground states approach a characteristic sequence of structures composed of radial grain boundaries ("neutral scars"), extending radially from the boundary and terminating in the bulk. Employing a combination of numerical simulations and asymptotic analysis of continuum elasticity theory, we prove that an energetic hierarchy gives rise to a structural hierarchy, whereby dislocation number and scar number diverge as $a/W \to 0$ while scar length and dislocation number per scar become *independent* of lattice spacing. We characterize a secondary transition occurring as scar length grows, where the n-fold scar symmetry is broken and ground states are characterized by polydisperse, forked-scar morphologies.

Understanding the ground-state order of curved, 2D crystals remains an outstanding challenge with far ranging implications, from the assembly of viral capsids [1,2] and multicomponent lipid membranes [3,4] to the structure and stability of particle coated droplets [5]. The planar, sixfold, equitriangular packing favored by isotropic interactions is incompatible with Gaussian curvature and as a consequence, topological defects are necessary features of ground-state order in curved crystals [6,7]. The importance of *disclinations*—points of localized five or sevenfold symmetry—has long been recognized for crystals on fixed-topology surfaces, like the well-known Thomson problem [8,9]. More recently, experimental [5,10], computational [11,12], and theoretical [13–15] studies have begun to recognize the importance of a related class of defects, *dislocations*—"neutral" five-seven dipoles—in the minimal-energy states of curved crystals, both with and without disclinations. Unlike disclinations, the number of dislocations, N_d, in curved-crystal ground states grows arbitrarily large in the continuum limit—where W/a, the ratio of crystal size to lattice spacing diverges—resulting in multi-dislocation chains, known as "scars" [5,13], that span large portions of the crystal. While heuristic arguments have been proposed to explain the scaling of the total number of dislocations with surface curvature [10,13], to date there is little understanding of precisely how defects are arranged in multidislocation ground states and what mechanical, geometric, and microscopic parameters govern these emergent structures.

In this Letter, we study a continuum elasticity model of crystalline caps bound to a spherical substrate to illuminate the emergent structure of mutlidislocation ground states in the continuum limit. A combination of numerical and asymptotic analysis prove that as $N_d \to \infty$, the arrangement approaches a characteristic pattern: n_s radially oriented scars extending from the crystal edge terminating in the bulk (Fig. 1). An energetic hierarchy underlies the structural hierarchy characterizing these states, which was recently argued [16] to parallel mechanisms of elastic pattern formation in wrinkled ultrathin films [17,18], whereby certain features of the defect pattern (N_d and scar length, ℓ_s) are encoded in the mechanics of the asymptotic limit of vanishing lattice spacing, while other
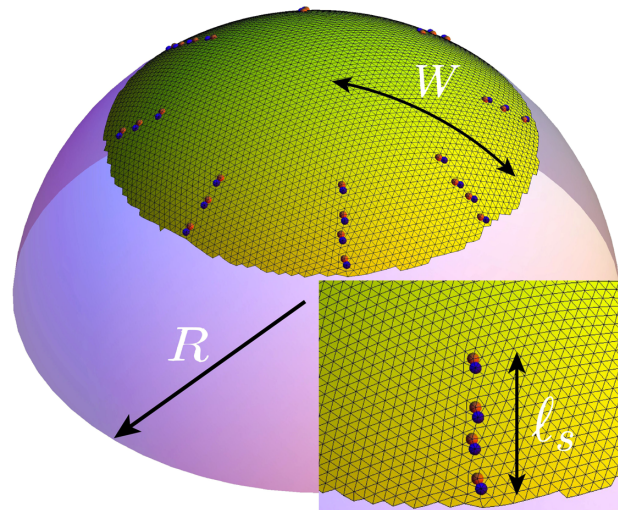

FIG. 1 (color online). Mesh reconstruction of an eight-scar ground state of a crystalline cap bound to sphere of radius R, where five-seven dislocation "dipoles" are shown as red (light) and blue (dark) vertices.

features (optimal scar number n_s) are governed by imperfect relaxation of geometric stresses by discrete dislocations. Here, we demonstrate that optimal symmetry of n-fold defect patterns is selected by a competition between the distinct energetics associated with different parts of the scars, their respective *lengths* and *ends*. Remarkably, this reveals that the asymptotic approach to the continuum limit is characterized by the divergence of *both* the number of *dislocations* and *scars*, such that N_d/n_s, the number of dislocations per scar, approaches a universal constant, independent of lattice spacing and defect core energy.

The influence of curvature on the structure of 2D crystals is complicated by several competing modes of relaxation triggered by geometrically induced stresses. These include i) "elastic" modes of out of plane shape deformation facilitated by patterns of wrinkles [16], crumples [18], and blisters [19], ii) shape instabilities of the free boundary of the solid domain [3,20,21], and iii) "plastic" reorganization of lattice packing facilitated by topologically "charged" or "neutral" arrays of defects [5,10,13]. To date, quantitative comparison of the relative efficacy of each mode to relax the cost of confinement has been hindered by the unknown structure and energetics of optimal defect patterns for $N_d \gg 1$. Here, to illuminate the underlying principles and quantitative accuracy emerging from the singular limit of "infinitely defective" crystals, we focus on the limiting parameter regime where the first two response types are suppressed by sufficiently large costs for substrate deformation or detachment [16] and boundary creation (e.g., large line tension) [20].

We study a circular 2D crystalline "cap" of radius W bound to a rigid spherical substrate of radius R, subject to an adhesive, radial tension T at its boundary that favors spreading of the cap over the substrate. Our analysis is based on the continuum elasticity theory of 2D crystals, where the total energy is

$$E = \frac{1}{2} \int dA \, \sigma_{ij} u_{ij} - T \Delta A. \tag{1}$$

For a weakly curved crystal, elastic strain derives from in-plane displacement $\mathbf{u}(\mathbf{x})$ (components in xy plane) and out-of-plane deflection $h(\mathbf{x})$, with $u_{ij} = (\partial_i u_j + \partial_j u_i + \partial_i h \partial_j h)/2$, while the stress response of a hexagonal crystal is characterize by Lamé constants, λ and μ, $\sigma_{ij} = \lambda \delta_{ij} u_{kk} + 2\mu u_{ij}$. The second term in Eq. (1) represents the adhesive work where $\Delta A = W \int d\theta u_r(r = W)$ is the area change of the sheet, and (r, θ) are polar coordinates. Dislocations are singular points, $\mathbf{x}_\alpha$, around which displacements increase (or decrease) by Burgers vector $\mathbf{b}$, corresponding to a partial row of lattice sites of width $|\mathbf{b}| \simeq a$ added or removed from crystal, terminating at $\mathbf{x}_\alpha$. For a curved crystal possessing dislocations [22], stress is governed by two relations, in-plane force balance, $\partial_i \sigma_{ij} = 0$, and the compatibility equation,

$$Y^{-1} \nabla_\perp^2 \sigma_{ii} = -K_G - \nabla_\perp \times \mathbf{b}(\mathbf{x}), \tag{2}$$

where $Y = 4\mu(\lambda + \mu)/(\lambda + 2\mu)$ is the 2D Young's modulus, $K_G = R^{-2}$ is the Gaussian curvature, and $\mathbf{b}(\mathbf{x}) = \sum_\alpha \mathbf{b}_\alpha \delta(\mathbf{x} - \mathbf{x}_\alpha)$ is the areal Burgers density. Note that in using Eq. (2), we assume the small-slope limit, where $|\nabla_\perp h| \approx W/R \ll 1$ and the cap covers a small (but finite) sphere fraction. In particular, we study coverages smaller than $(W/R)_c = \sqrt{2/3} \simeq 0.82$ beyond which small-slope theory is unstable to excess fivefold disclinations [23,24].

Stress in defect-free state, σ_{ij}^0, derives from geometric strains imposed by curvature and adhesive forces at the boundary, which require $\sigma_{rr}(r = W) = T$,

$$\sigma_{rr}^0 = \frac{Y}{16R^2}(W^2 - r^2) + T;$$

$$\sigma_{\theta\theta}^0 = \frac{Y}{16R^2}(W^2 - 3r^2) + T. \tag{3}$$

Unlike the radial direction which is always tensile, in the defect-free state for sufficiently small T, the hoop direction becomes compressive ($\sigma_{\theta\theta}^0 < 0$) at large radii, $r > L_0 = W/\sqrt{3}(1 + 2T/T_*)^{1/2}$, where $T_* = Y/8(W/R)^2$ is a critical tension above which the compressed zone vanishes. Dislocations corresponding to the removal of a row extending from the defect to the boundary (i.e., $\mathbf{b} = b\hat{\theta}$) relax compression at the edge and lower the elastic energy, provided their cost is sufficiently low. We characterize the susceptibility to dislocations (dubbed the "defectivity" of the crystal [16]) in terms of the ratio of dislocation self-energy, proportional to Yb^2, to elastic energy of the defect-free sheet, proportional to $YW^2(W/R)^4$,

$$\epsilon = (b/W)^2 (W/R)^{-4}, \tag{4}$$

which vanishes in the continuum limit $b/W \to 0$, indicating the instability of the crystal to dislocations when $T < T_*$. We study the structure and energy of multidislocation configurations in this regime by superposing σ_{ij}^0 with stresses generated by multiple dislocations ($\mathbf{b}$ aligned to hoop direction) [25]. The self-energy of dislocations, dislocation interaction energy, and the energy associated with relaxing geometrically induced compression derive from the free-boundary condition Greens functions of single dislocations [24,26] and Eq. (1) (see Supplemental Material [27]). For given values of tension, curvature and b/W, we relax the total energy by numerically adjusting defect position and number in the crystal. For fixed N_d, the energy is minimized by steepest descent starting from $\sim 10^4$ random initial defect configurations. The minimal energy multidislocation pattern is selected from this ensemble of "simulated quenches".

As T is reduced below T_*, a characteristic multidislocation pattern emerges: n_s evenly spaced and symmetric scars extending a distance ℓ_s from the edge into the cap. For conditions shown in Fig. 1 ($W = 0.3R$, $b = 0.013W$, $T = 0.1T_*$), we find a $n_s = 8$ scars of average length $\ell_s = 0.45W$, composed of $N_d = 27$ dislocations. While

optimal size and number of scars, as well as total defect number, change with both macroscopic (cap size, tension) and microscopic (Burgers vector) parameters, all simulated ground states show spontaneous emergence of n-fold symmetry at the onset of scar stability, $T \lesssim T_*$.

We now demonstrate how the features of this characteristic dislocation pattern are governed by the distribution of stress approached in the asymptotic limit $b/W \to 0$. The ultimate stress σ_{ij}^d of the defect-riddled state must be significantly remodeled by dislocations from the defect free stress σ_{ij}^0, which is unstable to defects. The stability of multidislocation state can be understood in terms of the Peach-Kohler force [28] acting on dislocations, $f_i = b\epsilon_{ij}\sigma_{j\theta}^d$, which implies that dislocations climbing from the boundary continue to lower the energy until defects are localized to regions where $\sigma_{r\theta}^d = \sigma_{\theta\theta}^d = 0$. The stable stress pattern derives from the continuum dislocation density $\mathbf{b}_c(\mathbf{x}) = b\rho(r)\hat{\theta}$ that approximates defect distribution in the $N_d \to \infty$, $b \to 0$ limit, and mechanical constraints imposed by a zone of vanishing compression [16]. The axisymmetry of the areal density $\rho(r)$ implies vanishing of shear stress, while the collapse of hoop stress is governed by the solution of Eq. (2) in two radial zones: a defect-free ($\rho = 0$) *axisymmetric inner region* for $r < L_d$, where the stress is identical to Eq. (3) up to an overall additive constant; and an *outer scarred zone* ($\rho \neq 0$) for $r \geq L_d$, where $\sigma_{\theta\theta}^d = 0$ as required by defect stability and $\sigma_{rr}^d = TW/r$ as required by force balance and boundary conditions. Continuity of radial and hoop components at the edge of scarred zone require an defect-free inner zone of radius

$$L_d = W - \ell_s = W(T/T_*)^{1/3}, \qquad (5)$$

which predicts that scars extend *beyond* the original compressed zone of the defect free state since $L_d < L_0$. Like the "far-from-threshold" analysis of wrinkling of ultrathin elastic sheets [16,18,29], the asymptotic stress pattern achieved in a defect-riddled cap in the $b/W \to 0$ limit is independent of "microscopic" features of the pattern, including b and the scar number, n_s.

Given this stable, compression-free pattern of stress, the dislocation distribution is determined by integrating the compatibility relation—matching the discontinuity in $\partial_r \sigma_{ii}^d$ at $r = L_d$ with the dislocation density at the edge of the scarred zone—yielding

$$\rho(r) = \frac{\epsilon^{-1/2}}{8W^2}\left[4\frac{r}{W} - \frac{T}{T_*}\left(\frac{W}{r}\right)^2\right]. \qquad (6)$$

Integrating $\rho(r)$ over the scarred zone $L_d \geq r \geq W$, the total dislocation number becomes,

$$N_d = \frac{\pi\epsilon^{-1/2}}{12}[4(1 - T/T_*) + (T/T_*)\ln(T/T_*)]. \qquad (7)$$

At small T, $N_d \sim \epsilon^{-1/2}$ is consistent with the balance of the total edge length removed by dislocations $N_d b$ and shortening of latitudes at the outer boundary imposed by spherical geometry $\sim W(W/R)^2$, while as $T/T_* \to 1$, boundary forces eliminate this compression; hence, the dislocation number vanishes in the limit $N_d \sim \epsilon^{-1/2}(T_* - T)$.

Notably, the principle of stress collapse in the scarred zone illustrated here is equivalent to the previously invoked notion of "perfect screening" of Gaussian curvature by dislocations which, for $T = 0$, achieves $\sigma_{ij} = 0$ throughout the sheet [10,13]. Comparison to numerical simulations demonstrates that the value of the "perfect screening" distribution, and its generalization to nonzero boundary forces, is far more than heuristic, describing certain features of multidislocation states (length of scars and defect number) quantitatively, even for finite, but large values of $\epsilon^{-1} \sim (W/b)^2$. In Figs. 2(a)–2(b), we compare predictions for ℓ_s and N_d to "free dislocation" simulations, as well as to a much larger class of numerically optimized, fixed n-fold symmetry radial scar patterns, whose fewer degrees of freedom (radial positions of each dislocation
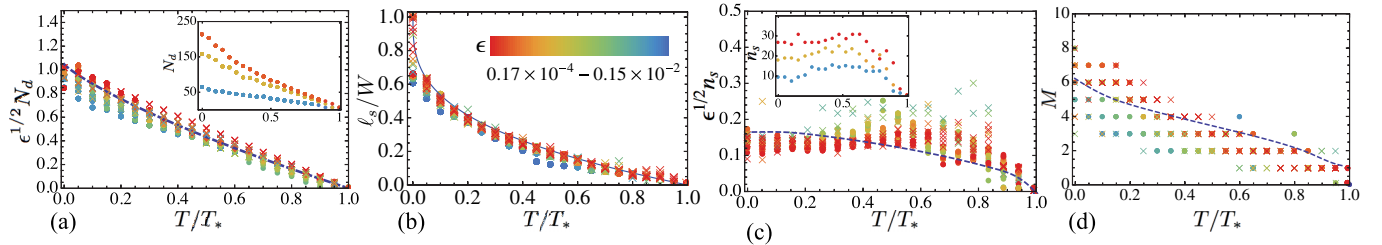

FIG. 2 (color online).   The scaled dislocation number $\epsilon^{1/2}N_d$ (a), the length of the scarred zone ℓ_s (b), the scaled scar number $\epsilon^{1/2}n_s$ (c), and the number of dislocations per scar M (d) for simulated ground states of the cap are shown as functions of the reduced tension, T/T_*. Insets of (a) and (c) are unscaled dislocations and scar numbers. Results from unconstrained, "free dislocation" and imposed n-fold symmetric simulations are shown, respectively, as crosses and filled circles. Color scale of points in (b) correspond to dimensionless dislocation cost $\epsilon = (b/W)^2(W/R)^{-4}$, where simulations were carried out over a range of cap sizes and curvatures: $W/b = 100$–1400 and $W/R = 0.05$–0.3. The dashed lines indicate predictions from asymptotic analysis of dominant and subdominant energetics of defect patterns.

"ring" allow us to reach highly "defective" caps, up to $\epsilon^{-1} \simeq 6 \times 10^4$ and $N_d \approx 250$.

Unlike the dislocation number and scar length, the optimal scar number does not derive from the asymptotic stress pattern σ_{ij}^d in the $b/W \to 0$ limit, which is independent of n_s. In [16], it was shown in the limit of narrow scars ($\ell_s/W \ll 1$) that the n_s-degenerate energetics encoded in the elastic energy of asymptotic stress σ_{ij}^d correspond directly to the combination of relaxation energy per scar and the repulsive interactions between scars, which describe, respectively, the dominant gains and costs of multiscar patterns. Here, we consider *subdominant* costs of the self-energies of scars, in terms of distinct costs attributed to the *ends* and *lengths* of scars, which describe energetics of fine-scale (intrascar) stresses absent from the continuum limit, and more important, lift the degeneracy of the energy with n_s.

Scars differ from ordinary grain boundaries in that the former terminate in the bulk of crystal [13]. Crossing a grain boundary implies rotation of crystal axes by b/D, where D is the dislocation spacing. Hence, scar ends are disclinationlike singularities, points around which lattice directions rotate rapidly [28], and the far-field stresses generated by scars are dominated by these end singularities. Estimating dislocation spacing as $D = \ell_s n_s / N_d$ yields an effective disclination charge $s \approx b/D \sim (b/\ell_s)(N_d/n_s)$, and the elastic cost to introduce this charge $\ell_s \approx W$ from the cap edges becomes $\sim Y s^2 W^2$ [22]. In addition to the cost of the singular ends, grain boundary scars are characterized by a "line tension" $\sim Y b^2 / D[\ln(D/b) + E_c]$ [28], where E_c parameterizes the inelastic core energies of dislocations, from which we estimate

$$E_{\text{self}} \approx n_s^{-1} Y (N_d b/W)^2 + Y b^2 N_d \ln\left(\frac{N_d W}{n_s b'}\right)$$
$$\sim E_0[n_s^{-1} + \epsilon^{1/2} \ln(n_s \epsilon^{1/2})], \qquad (8)$$

where b' is a renormalized core size and $E_0 \approx Y(W/R)^4 W^2$. The elastic cost of scar tips favors a large number of low-angle scars, which is balanced by the weaker ($\propto \epsilon^{1/2}$) preference of line tension for dense scars (small n_s). This sets an optimal scar number $n_s \sim \epsilon^{-1/2} \gg 1$ that diverges in the continuum limit as $W/b \to \infty$. As the dislocation number and scar length vary with T/T_*, we expect more generally that optimal scar number of n_s-fold symmetric states behaves as

$$n_s = \epsilon^{-1/2} \bar{n}_s(T/T_*), \qquad (9)$$

where $\bar{n}_s(x)$ is dimensionless function which vanishes as $x \to 1$. Assuming n-fold symmetry for all T, we may determine $\bar{n}_s(T/T_*)$ by numerically optimizing self-energy contributions for all T/T_* (see Supplemental Material [27]). This prediction for optimal scar number is compared to numerical ground states (both n-fold and "free dislocation"

simulations) in Fig. 2(c), confirming the collapse of optimal scar number to form of Eq. (9) as $\epsilon \to 0$. Both dislocation and scar number diverge as $\epsilon^{-1/2}$, implying a universality in the approach to the continuum distribution of dislocations. Remarkably, the number of dislocations per scar $N_d/n_s \equiv M(T/T_*)$ is predicted to approach a constant value for a given ratio T/T_*, *independent* of lattice spacing. As shown in Fig. 2(d), M varies weakly with tension, from $M \simeq 1$ as $T \to T_*$, to roughly six dislocations per scar in the absence of boundary forces ($T = 0$).

We conclude with an analysis of the symmetry of scar patterns in our "free dislocation" simulations (e.g., defect positions not constrained to n-fold patterns) examples of which are shown in the range $0 \leq T < T_*$ in Fig. 3. We quantify the degree of n-fold symmetry in terms of the angular transform of simulated dislocation positions, $\bar{\rho}_m = \int dA e^{im\theta} \rho(\mathbf{x})$, and analyze the relative amplitudes of the principle nonzero mode $m = n_s$—which serves as definition of scar number of "free dislocation" simulations—compared to higher harmonics of the distribution, $m = k n_s$. Identical, evenly spaced scars imply $|\bar{\rho}_{n_s}| = |\bar{\rho}_{2n_s}| = |\bar{\rho}_{3n_s}| = \ldots$, and therefore, we define $S \equiv |\bar{\rho}_{2n_s}|/|\bar{\rho}_{n_s}|$ as a measure of perfect n-fold symmetry. Figure 3(g) shows the variation of n-fold symmetry S with boundary tension and susceptibility to defects, ϵ^{-1}. Significantly, for sufficiently large tension ($T \lesssim T_*$), simulated ground states retain high-symmetry, characterized by $S \simeq 1$. Decreasing T for fixed ϵ^{-1}, we find an abrupt transition to $S \ll 1$, indicating marked loss of n-fold symmetry, coincident with the appearance of polydisperse or forked, scar morphologies observed for $T \to 0$ [Figs. 3(a)–3(c)]. Our simulations suggest that in the continuum limit ($\epsilon \to 0$), n-fold symmetric dislocation patterns become unstable to a lower symmetry, multiscale pattern for $T \lesssim 0.4 T_*$, or equivalently, when the length of scarred zone exceeds a critical value, $\ell_s \gtrsim 0.3W$.

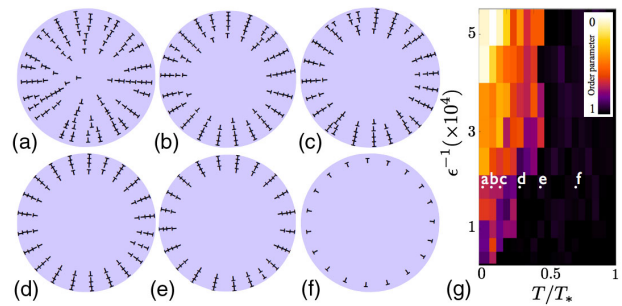While we relegate a detailed study of this structural instability to a future publication [30], comparison of

FIG. 3 (color online). (a)–(f) free-dislocation ground states for a sequence of increasing tension, with parameter values shown in (g), a map of n-fold symmetry of dislocation pattern as measured by order parameter S (defined in text), with dark and light colors showing regions of n-fold symmetric and polydisperse, forked-scar patterns, respectively.

the stress and energy of ground-state patterns (see Supplemental Material [27]) suggests that transition from n-fold to "forked scar" patterns in our simulations is consistent with a transition in the *subdominant energetics* associated with fine-scale variations in the elastic energy, rather than a reorganization of the dominant stress distribution. As a consequence, those features of the dislocation pattern determined by this asymptotic stress (as $\epsilon \to 0$), the scar length, and dislocation number, are not altered by the loss of n-fold symmetry, as we observe in Figs. 2(a)–2(b). Moreover, the "scar number" of forked-scar patterns as measured by the primary mode number of $\bar{\rho}_m$ follows the same data collapse in terms of T/T_* and ϵ implied by Eq. (9) for n-fold symmetric patterns [Figs. 2(c)–2(d)], highlighting the more general applicability of the structural and energetic hierarchy for controlling defect patterns beyond conditions of idealized symmetry.

The emergence of a characteristic structure and energetics of multidislocation patterns in the continuum limit of $b/W \to 0$ yeilds new predictions for the symmetries of observable scar patterns formed on particle-coated liquid intefaces in the poorly characterized shallow-curvature regime [10], and it opens the door to a broader and more rigorous understanding of the role of "plastic" modes of curved-crystal relaxation beyond this particular limit (small area coverage, larger boundary tension, rigid substrate). For example, it has been shown [16] for flexible crystals bound to deformable spherical substrates that the pattern of "elastic" deformation triggered by confinement (radial wrinkles) achieves the *identical* state of asymptotic stress for $T \lesssim T_*$. Hence, the relative stability of plastic versus elastic response to curvature is determined purely by the respective subdominant costs of either mode, which reveals a nontrivial transition from wrinkles to scars with increasing geometric compression. Beyond small curvature, ongoing work is considering how the appearance of excess disclinations restructure the underlying dominant stress distribution of highly curved caps, and thereby alter the consequences of multidislocation stress collapse relevant to 1) optimal symmetries of multidislocation scars that decorate "charged" disclinations of close spherical shells [5,13] (e.g., the Thomson problem) and 2) the curvature-driven transition from "uncharged" to "charged" dislocations scars on crystalline caps.

[1] D. L. D. Caspar and A. Klug, Cold Spring Harbor Symp. Quant. Biol. **27**, 1 (1962).

[2] R. Zandi, D. Reguara, R. F. Bruinsma, W. M. Gelbart, and J. Rudnick, Proc. Natl. Acad. Sci. U.S.A. **101**, 15556 (2004).

[3] S. Schneider and G. Gompper, Europhys. Lett. **70**, 136 (2005).

[4] G. Vernizzi, R. Sknepnek, and M. Olvera de la Cruz, Proc. Natl. Acad. Sci. U.S.A. **108**, 4292 (2011).

[5] A. R. Bausch, M. J. Bowick, A. Cacciuto, A. D. Dinsmore, M. F. Hsu, D. R. Nelson, M. G. Nikolaides, A. Travesset, and D. A. Weitz, Science **299**, 1716 (2003).

[6] M. Kléman, Adv. Phys. **38**, 605 (1989).

[7] J.-F. Sadoc and R. Mosseri, *Geometrical Frustration* (Cambridge University Press, Cambridge, 1999).

[8] E. L. Altschuler, T. J. Williams, E. R. Ratner, F. Dowla, and F. Wooten, Phys. Rev. Lett. **72**, 2671 (1994).

[9] M. Bowick, A. Cacciuto, D. R. Nelson, and A. Travesset, Phys. Rev. Lett. **89**, 185502 (2002).

[10] W. T. Irvine, V. Vitelli, and P. M. Chaikin, Nature (London) **468**, 947 (2010).

[11] D. J. Wales, H. McKay, and E. L. Altschuler, Phys. Rev. B **79**, 224115 (2009).

[12] H. Kusumaatmaja and D. J. Wales, Phys. Rev. Lett. **110**, 165502 (2013).

[13] M. J. Bowick, D. R. Nelson, and A. Travesset, Phys. Rev. B **62**, 8738 (2000).

[14] A. Travesset, Phys. Rev. B **68**, 115421 (2003).

[15] V. Vitelli, J. B. Lucks, and D. R. Nelson, Proc. Natl. Acad. Sci. U.S.A. **103**, 12323 (2006).

[16] G. M. Grason and B. Davidovich, Proc. Natl. Acad. Sci. U.S.A. **110**, 12893 (2013).

[17] E. Cerda and L. Mahadevan, Phys. Rev. Lett. **90**, 074302 (2003).

[18] H. King, R. D. Schroll, and B. Davidovich, Proc. Natl. Acad. Sci. U.S.A. **109**, 9716 (2012).

[19] J. Hure, B. Roman, and J. Bico, Phys. Rev. Lett. **106**, 174301 (2011).

[20] A. Y. Morozov and R. F. Bruinsma, Phys. Rev. E **81**, 041925 (2010).

[21] G. Meng, J. Paulose, D. R. Nelson, and V. N. Manoharan, Science **343**, 634 (2014).

[22] D. R. Nelson, *Defects and Geometry in Condensed Matter Physics* (Cambridge, Cambridge, 2002).

[23] G. M. Grason, Phys. Rev. Lett. **105**, 045502 (2010).

[24] G. M. Grason, Phys. Rev. E **85**, 031603 (2012).

[25] As the *density* of defects in the ground state patterns vanishes as $\sim b/W$ in the continuum limit, we neglect corrections due to nonlinear elastic effects arising at small interdefect spacing.

[26] A. Azadi and G. M. Grason, Phys. Rev. E **85**, 031604 (2012).

[27] See Supplemental Material at http://link.aps.org/supplemental/10.1103/PhysRevLett.112.225502 for details on the effective theory of multidislocation caps and numerical methods for ground-state patterns.

[28] J. P. Hirth and J. Lothe, *Theory of Dislocations* (Wiley, New York, 1982).

[29] B. Davidovich, R. D. Schroll, D. Vella, M. Adda-Bedia, and E. A. Cerda, Proc. Natl. Acad. Sci. U.S.A. **108**, 18227 (2011).

[30] A. Azadi and G. M. Grason (to be published).